Rheo-Optical Studies of Shear-Induced Structures in Semidilute Polystyrene Solutions

Takuji Kume† and Takeji Hashimoto*

Department of Polymer Chemistry, Graduate School of Engineering, Kyoto University, Kyoto 606-01, Japan

Tsutomu Takahashi

Department of Mechanical Engineering, Nagaoka University of Technology, Nagaoka, Niigata, Japan

Gerald G. Fuller

Department of Chemical Engineering, Stanford University, Stanford, California 94305-5025

Received April 30, 1997; Revised Manuscript Received September 4, 1997[⊗]

ABSTRACT: Shear-induced structure formation in semidilute solutions of high molecular weight polystyrene (PS) was investigated by rheology, shear-dichroism, shear-birefringence, shear-small-angle light-scattering (SALS) and shear-optical-microscopy methods. At the shear rate $\dot{\gamma}_c < \dot{\gamma} < \dot{\gamma}_a$, where $\dot{\gamma}_c$ and $\dot{\gamma}_a$ are the critical shear rates for the onset of the shear-enhanced concentration fluctuations and the onset of the anomalies in the rheological and scattering behaviors respectively, we observed negative dichroism, almost zero birefringence, and butterfly type LS patterns. All these results are consistent with the optical images captured by shear-microscopy and show the shear-induced concentration fluctuations with the following characteristics: the amplitude of the fluctuations is enhanced along the flow direction, and the domain structure (regions rich in polymer concentration) formed is extended normal to flow. However, at the shear rate $\dot{\gamma} > \dot{\gamma}_a$, the dichroism became positive and the absolute values of both the dichroism and the birefringence increased drastically. The changes in the dichroism and the birefringence are believed to be related to formation of the stringlike structures and molecular orientation both parallel to flow.

I. Introduction

In recent years the shear-induced structure formation in polymeric systems have attracted a great deal of attention, and many experimental and theoretical studies of shear-induced concentration fluctuations or phase separation in semidilute polymer solutions have been reported.[1−33] In order to investigate this phenomenon, several experimental methods, such as rheology,[12,13,15,24−27,31−33] transmitted light intensity,[2−4,19] shear-dichroism,[12,17,19,20,24,26,32] shear-small-angle light scattering,[8,9,11,12,15−21,23−31,33] shear-small-angle neutron scattering,[22] and shear-optical microscopy[21,25,28−30,33] have been used.

Our previous studies[9,15,21,23,27,33] revealed that the effects of shear on the semidilute polymer solutions could be classified into some regimes with respect to shear rate $\dot{\gamma}$: homogenous solution at $\dot{\gamma} < \dot{\gamma}_c$; shear-induced concentration fluctuations at $\dot{\gamma}_c < \dot{\gamma} < \dot{\gamma}_a$ which cause the strong butterfly-type light scattering pattern; the anomalies in the rheological and scattering behaviors at $\dot{\gamma} > \dot{\gamma}_a$, which are related to streaklike scattering pattern and string phase in microscopic images. Here $\dot{\gamma}_c$ and $\dot{\gamma}_a$ are the critical shear rates for the onset of the shear-enhanced concentration fluctuations and for the onset of the anomalies in the rheological and scattering behaviors, respectively. The basic concept which explains the origin of the butterfly patterns has been well developed by recent theories[5−7,10,13,14] based on the nonequilibrium statistical mechanics: The butterfly patterns or anisotropic concentration fluctuations are induced by a coupling between concentration fluctuations and stress existing in the system as a result of the concentration dependence of viscosity and normal stress coefficients (the so-called elastic effects). Important future studies would involve quantitative interpretations of experimental results with the theories. On the other hand, the transition of the scattering pattern from the butterfly pattern to the streaklike pattern at $\dot{\gamma}_a$ has not been accounted for at all by the present theories.

In this paper we focus on the construction of a more complete picture of the shear-induced phase separation and structure formation by systematically comparing the results from a wide range of techniques on the same polymer solutions: rheological experiments, form dichroism, birefringence, light scattering, and optical microscopy. This is in contrast to previous reports using a limited number of rheo-optical techniques used separately for different systems.

II. Experimental Method

II-A. Samples. The three polymer solutions used in this study consist of high molecular weight polystyrene (PS) dissolved in dioctyl phthalate (DOP). DOP is a Θ solvent for PS, and its Θ temperature (T_Θ) is 22 °C.[34] Characterizations of the PS and their solutions are listed in Table 1. Concentrations of our solutions are in the semidilute regime. The methods used to prepare them are same as those used in previous experiments.[8,9,15]

The PS/DOP system has a phase diagram of the UCST-type. Cloud points of three samples exist in the temperature range 10−16.3 °C. All the samples are in a one-phase region in the quiescent state at experimental temperature (PS548/DOP, 22 °C; PS384/DOP, 21 °C).

II-B. Shear-Dichroism, Birefringence, and Rheology Figure 1 shows the experimental system used to measure the dichroism and birefringence of the solutions under shear flow.

* To whom correspondence should be addressed.
† Present address: Kao Corporation, Tokyo Research Laboratory, 1-3, Bunka 2-chome, Sumida-ku, Tokyo, 131 Japan.
⊗ Abstract published in *Advance ACS Abstracts,* October 15, 1997.

S0024-9297(97)00598-6 CCC: $14.00

Table 1. Polymer Solutions Used in This Work

polymer code	M_w[a] ($\times 10^{-6}$)	M_w/M_n[b]	concentration (wt %)	c/c^* [b]	cloud point[c] (°C)
PS548	5.48	1.15	3.0	≈20	16.3
PS548	5.48	1.15	6.0	≈40	13.8
PS384	3.84	1.06	6.0	≈30	10

[a] M_w and M_n are weight-average molecular weight and number-average molecular weight, respectively. [b] c*: overlap concentration. [c] The cloud points of the PS548 and PS384 solutions were determined by the same method as described elsewhere.[8,9,15]

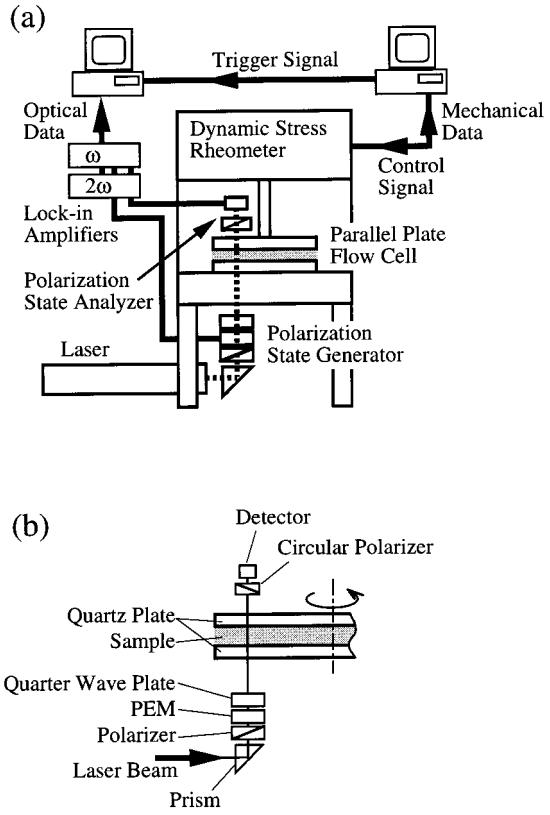

Figure 1. Schematic diagram of the experimental setup for shear-dichroism, shear-birefringence, and rheology: (a) Schematic diagram of the combined mechanical rheometer and optical train. (b) Shear cell and optical train.

A Rheometrics dynamic stress rheometer (DSR) serves as the mechanical platform. The sample is contained between two quartz disks that form a parallel plate shear cell. The upper plate is rotated to induce shear. The optical train is situated below the rheometer and light is directed through the sample at normal incidence. The optical train below the shear cell consists of a He−Ne laser, followed by a prism, a photoelastic modulator and a quarter-wave plate. The transmitted light is received by a detector either in a direct form (for dichroism measurements) or after passing through a circular polarizer (for birefringence measurements). Details of this measurement technique were reported elsewhere.[24,32]

II-C. Shear-Light Scattering. Small-angle light-scattering measurements under shear flow (shear−small-angle light scattering, shear-SALS) are carried out in the same way as we performed previously[9,15,27,29,33] with the rheo-optical apparatus described in detail elsewhere.[35] Figure 2 shows a schematic diagram for the optical setup and the coordinate system used in this study. The sample cell is a transparent cone-and-plate type shear cell, and made of quartz with 80 mm diameter and 1° cone angle.

A He−Ne CW gas laser ($\lambda_0 = 632.8$ nm, 15 mW) and a 35-element photodiode array are used as an incident beam source and a one-dimensional detector, respectively, for quantitative measurements of the scattered intensity distributions from the sheared solutions.

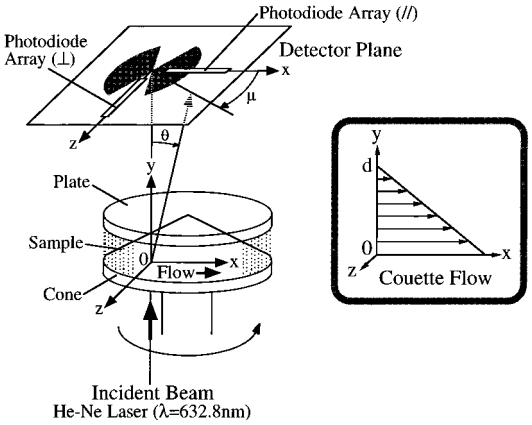

Figure 2. Schematic diagram of the experimental setup for shear-light scattering: one-dimensional detector (photodiode array), cone-and-plate type shear cell to generate Couette flow, and coordinate system used in this study. Note that the coordinate system used here is identical to that commonly used in this field but is different from the one we used in our earlier work,[8,9,15,21,25,35] which is based on a tradition in the field of scattering.

The light scattering intensity profile $I(q_x,q_z)$ was measured in the plane Oxz, where q_x and q_z are the x and z components (i.e. $\mu = 0$ and 90°, respectively) of the scattering vector **q** whose magnitude q is related to the wavelength λ of the incident beam and the scattering angle θ in the solution by

$$q = (4\pi/\lambda)\sin(\theta/2) \tag{1}$$

Furthermore, we investigated the shear-induced phase separation by measuring integrated scattering intensities, $F_{\parallel}(\dot\gamma)$ and $F_{\perp}(\dot\gamma)$, parallel and perpendicular to the flow direction, respectively, as a function of shear rate $\dot\gamma$. They are defined by

$$F_{\parallel} = \int_{a_2}^{a_1} dq_x \int_{-\delta}^{\delta} dq_z I(q_x,q_z) \tag{2}$$

and

$$F_{\perp} = \int_{a_2}^{a_1} dq_z \int_{-\delta}^{\delta} dq_x I(q_x,q_z) \tag{3}$$

The quantity δ is the magnitude of the scattering vector (3.4×10^{-5} nm^{-1}) which is subtended by the height of the slit placed in front of the photodiode array, and a_1 and a_2 were set at 6.2×10^{-4} nm^{-1}, and 2.7×10^{-3} nm^{-1}, respectively. Furthermore we used photographic films, which were set in the plane Oxz, for observation of qualitative two-dimensional light scattering patterns.

Our modified DSR does not have a temperature-control system. On the other hand the shear-light-scattering apparatus has a double-chambered temperature enclosure.[33] Thus in this study, the sample temperature was controlled at the temperature where the experiments with the modified DSR apparatus were conducted (e.g. 21 or 22 °C) with accuracy of ±0.2 °C at the incident beam spot.

III. Results

Figure 3 shows the plots of shear rate ($\dot\gamma$), birefringence ($\Delta n'$), and dichroism ($\Delta n''$) values for the PS548/DOP 3.0 wt % solution as a function of shear stress (σ) measured by using the modified DSR. These three measurements were separately carried out. The DSR is a stress-controlled type rheometer; thus, our modified DSR can measure these data under the steady shear flow at a given shear stress. These measurements were also carried out similarly for other two solutions. However, the shear-light-scattering data were measured as a function of shear rate as described in the previous study.[9,15,27,29,33] Therefore birefringence and

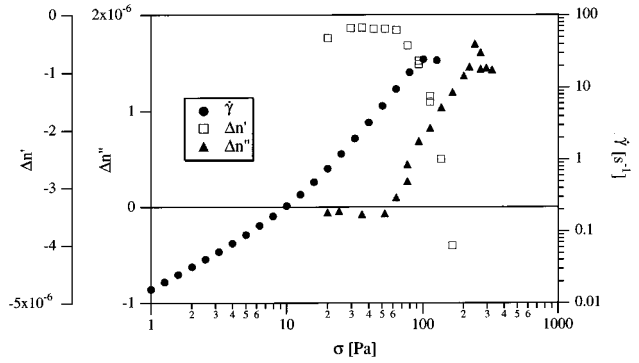

Figure 3. Plots of shear rate ($\dot{\gamma}$), birefringence ($\Delta n'$), and dichroism ($\Delta n''$) for the PS548/DOP 3.0 wt % solution at room temperature (22 °C) as a function of shear stress (σ).

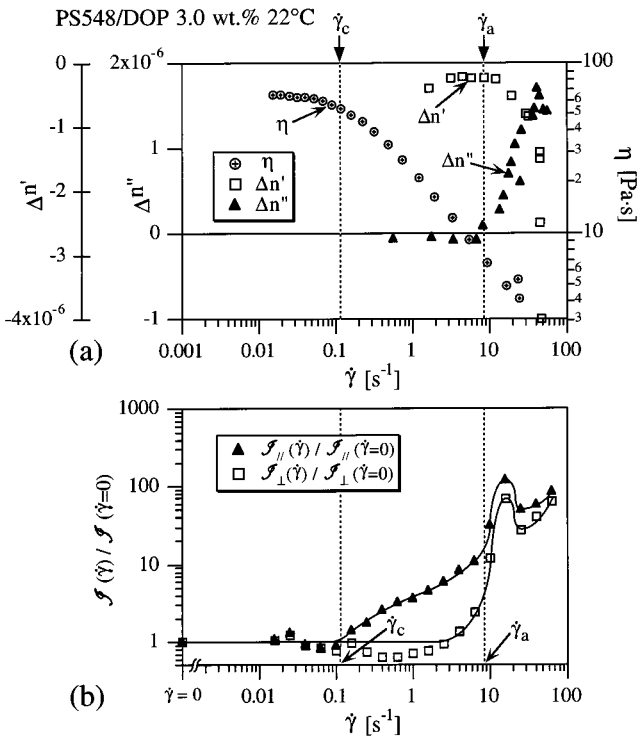

Figure 4. Sample solution used for this figure is PS548/DOP 3.0 wt % at 22 °C: (a) the plots of shear viscosity (η), birefringence ($\Delta n'$), and dichroism ($\Delta n''$) of this solution as a function of shear rate ($\dot{\gamma}$), which were calculated from the data as shown in Figure 3; (b) the plots of $F_{\parallel}(\dot{\gamma})/F_{\parallel}(\dot{\gamma} = 0)$ and $F_{\perp}(\dot{\gamma})/F_{\perp}(\dot{\gamma} = 0)$, integrated scattered intensity at a given $\dot{\gamma}$, normalized with respect to the integrated intensity of the quiescent solution, parallel and perpendicular to the flow direction, respectively.

dichroism data were replotted as a function of shear rate in parts a of Figures 4−6 in comparison with light scattering data. Furthermore shear viscosity (η) data, as estimated by

$$\eta = \sigma/\dot{\gamma} \tag{4}$$

were also included in these figures.

Figures 4−6 show the results of the PS548/DOP 3.0 wt % solution, the PS548/DOP 6.0 wt % solution, and the PS384/DOP 6.0 wt % solution, respectively. Parts a of these figures are the plots of η, $\Delta n'$ and $\Delta n''$ of each solution as a function of shear rate ($\dot{\gamma}$). Parts b of them are plots of $F_{\parallel}(\dot{\gamma})/F_{\parallel}(\dot{\gamma} = 0)$ and $F_{\perp}(\dot{\gamma})/F_{\perp}(\dot{\gamma} = 0)$, with integrated scattered intensity parallel and perpendicular to the flow direction, respectively, at a given $\dot{\gamma}$, normalized with respect to the integrated intensity of

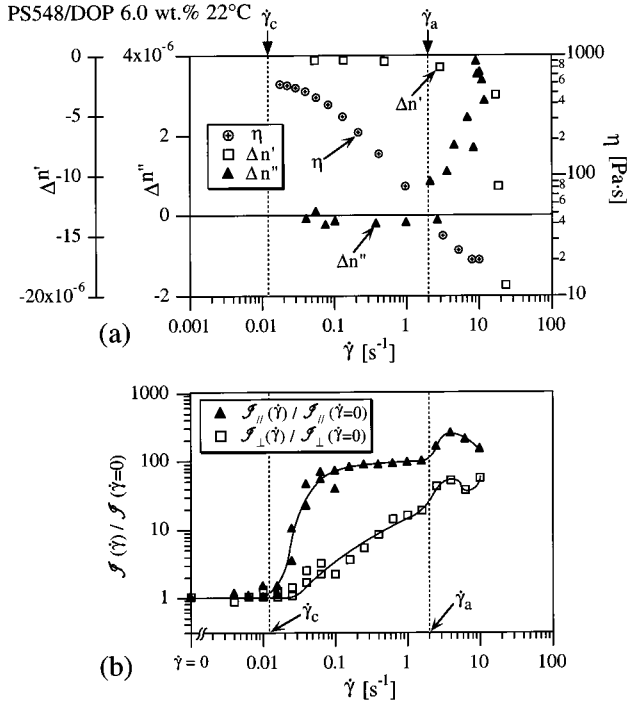

Figure 5. Sample solution used for this figure is PS548/DOP 6.0 wt % at 22 °C. (a) The plots of shear viscosity (η), birefringence ($\Delta n'$), and dichroism ($\Delta n''$) of this solution as a function of shear rate ($\dot{\gamma}$). (b) The plots of $F_{\parallel}(\dot{\gamma})/F_{\parallel}(\dot{\gamma} = 0)$ and $F_{\perp}(\dot{\gamma})/F_{\perp}(\dot{\gamma} = 0)$, integrated scattered intensity at a given $\dot{\gamma}$, normalized with respect to the integrated intensity of the quiescent solution, parallel and perpendicular to the flow direction, respectively.

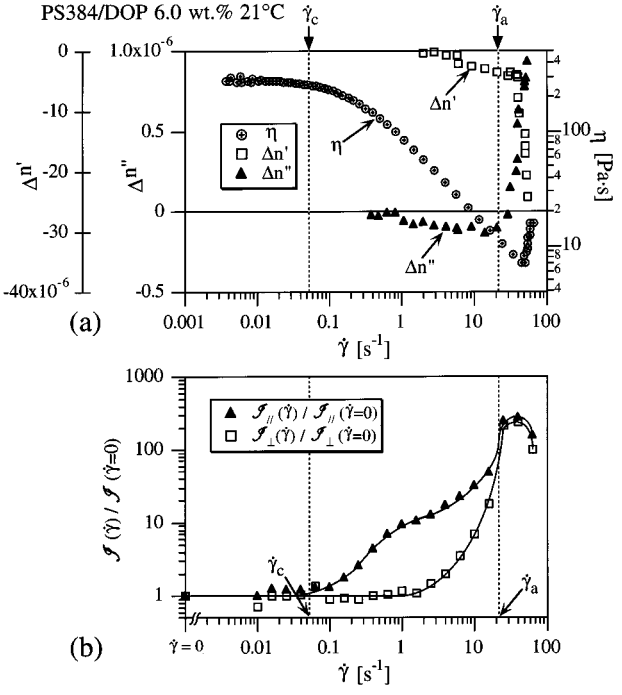

Figure 6. Sample solution used for this figure is PS384/DOP 6.0 wt % at 21 °C. (a) The plots of shear viscosity (η), birefringence ($\Delta n'$), and dichroism ($\Delta n''$) of this solution as a function of shear rate ($\dot{\gamma}$). (b) The plots of $F_{\parallel}(\dot{\gamma})/F_{\parallel}(\dot{\gamma} = 0)$ and $F_{\perp}(\dot{\gamma})/F_{\perp}(\dot{\gamma} = 0)$, integrated scattered intensity at a given $\dot{\gamma}$, normalized with respect to the integrated intensity of the quiescent solution, parallel and perpendicular to the flow direction, respectively.

the quiescent solution. Furthermore Figure 7 shows the small-angle light-scattering patterns of the PS384/DOP 6.0 wt % solution at 21 °C, which were simultaneously

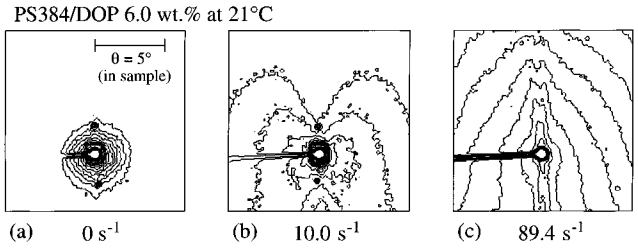

Figure 7. Contour plots of the scattered intensity distribution for steady state scattering patterns at various shear rates for the solution shown in Figure 6.

taken with the experiments of Figure 6. These patterns represent contour plots showing the iso-intensity levels. In the construction of the contour patterns, we first scanned the scattered intensity recorded on photographic films with an intensity scanner, and then smoothed the intensity fluctuations in the original scattering patterns which arise from the speckled patterns.

The results on three solutions in Figures 4−6 showed the same tendency, except for the shifts of the critical shear rates $\dot{\gamma}_c$ and $\dot{\gamma}_a$ with varying concentrations and molecular weights of polystyrene. It is extremely important to note that we could obtain similar results on the solutions with different concentrations and molecular weights, because it suggests that these transitions under shear flow are quite universal phenomena. First, parts b of Figures 4−6 indicate that shear rate dependence of the integrated scattering intensity, especially along the flow ($F_{\parallel}(\dot{\gamma})/F_{\parallel}(\dot{\gamma}=0)$), can be classified into several regimes as we reported previously.[15,27,29,33] For each solution there are two critical shear rates, the critical shear rate for the shear-enhanced concentration fluctuations or phase-separation ($\dot{\gamma}_c$) and the second critical shear rate or the critical shear rate for the onset of the anomalous behavior ($\dot{\gamma}_a$). Furthermore behavior of the shear viscosity in part a is also classified into the same regimes.

At $\dot{\gamma} < \dot{\gamma}_c$, the scattering intensity was essentially identical to those of homogeneous semidilute solutions as seen in Figure 7a, and shear viscosity is almost constant with $\dot{\gamma}$; i.e., the solution appears to be almost a Newtonian fluid. At $\dot{\gamma}_c < \dot{\gamma} < \dot{\gamma}_a$, the scattering intensity increased and the shear viscosity decreased with increasing shear rate. Moreover, in this regime we could observe the unique butterfly-type scattering pattern[15,21,25,27,29,33] as seen in Figure 7b. At $\dot{\gamma} > \dot{\gamma}_a$, the scattering intensity further increased and the butterfly pattern changed into a strong streaklike pattern oriented perpendicular to the flow as seen in Figure 7c (the tendency being especially remarkable at high shear rates in this regime[27]). This strong streaklike pattern appeared at small-angle regions, and it was superposed on the elongated two-point pattern at large q regions which appeared parallel to flow, though the elongated two-point pattern is less distinct in Figure 7c than that in Figure 3g and 7 of ref 27. These anomalies in the change of the scattering pattern with $\dot{\gamma}$ were closely related to anomalies in rheological behavior: shear viscosity began to increase in this regime.

Next, the birefringence ($\Delta n'$) and dichroism ($\Delta n''$) at $\dot{\gamma} < \dot{\gamma}_c$ were too small to be detected with enough accuracy for our DSR. All three solutions indicated that the values of both the dichroism and the birefringence were negative and small at $\dot{\gamma}_c < \dot{\gamma} < \dot{\gamma}_a$ and that the dichroism changed sign with its value increasing with $\dot{\gamma}$ and the birefringence negatively increased drastically with $\dot{\gamma}$ at $\dot{\gamma} > \dot{\gamma}_a$.

IV. Discussion

The scattering pattern and intensity change together with the previous *in situ* observation with the optical microscopy under shear flow[21,25,27,33] reveal that the structure formation or the enhancement of concentration fluctuations depends on the shear rate $\dot{\gamma}$ as summarized in Figure 8. At $\dot{\gamma} < \dot{\gamma}_c$, only weak thermal concentration fluctuations exist in the solution, which are essentially identical to those of homogeneous semidilute solutions in the quiescent state (Figure 8a). At $\dot{\gamma}_c < \dot{\gamma} < \dot{\gamma}_a$, the elastic effect is significant, which develops the concentration fluctuations enhanced along flow and extended normal to flow, as evidenced by the shear-microscopy result (Figure 8b,c) or as schemati-

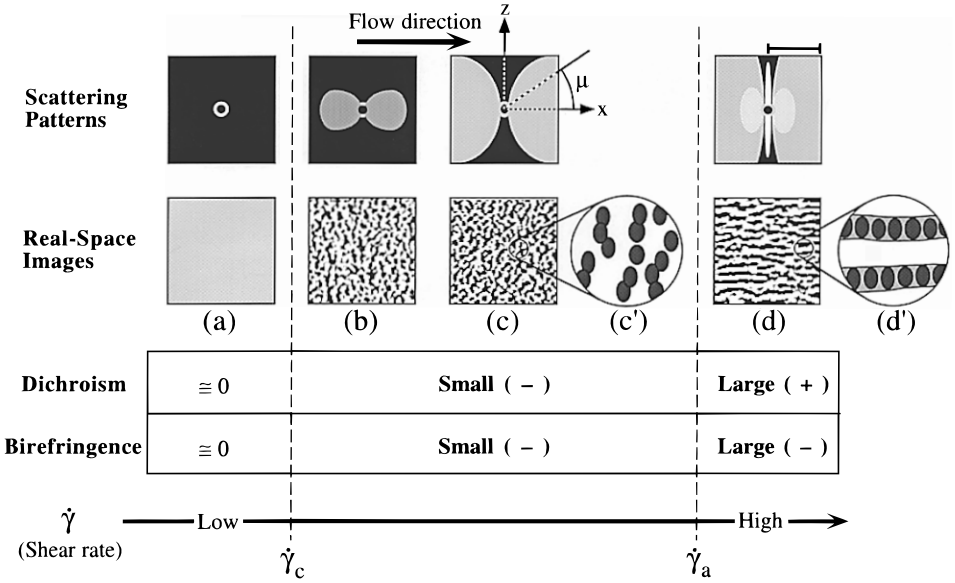

Figure 8. Schematic representation of the small-angle light-scattering patterns and concentration fluctuations observed in real space, i.e., by using optical microscopy, and a table of behaviors in dichroism and birefringence under steady shear flow at various shear rates. A scale bar on the top of part d indicates ca. 5° in the scattering angle, and length scale of the real-space images ca. 50 μm. The critical shear rates, $\dot{\gamma}_c$ and $\dot{\gamma}_a$, should depend on concentration and molecular weight and be referred to Figures 4−6. Parts c′ and d′ are enlarged models in part c and d, respectively.

cally shown in Figure 8c′.[36] This result is consistent with the butterfly pattern and the negative form dichroism. The birefringence is small and negative, suggesting that polystyrene chains only weekly orient along the flow direction.

However, at $\dot{\gamma} > \dot{\gamma}_a$ the shear-microscopy showed formation of long stringlike structures oriented along the flow (Figure 8d). This observation is consistent with the streaklike LS pattern oriented normal to flow and positive form dichroism. Namely, the structure transformation from the oblate-ellipsoidal structures with their axes preferentially oriented along flow to the stringlike structures with $\dot{\gamma}$ across $\dot{\gamma}_a$ causes the change of the sign and the absolute value of form-dichroism. The positive value of dichroism increases with $\dot{\gamma}$, revealing that the spatial correlation length of the strings along flow increases with $\dot{\gamma}$.

Although the previous experimental methods did not clarify the molecular orientation, the shear−birefringence results (the large negative values) indicate that the polymer molecules oriented strongly with their end-to-end vectors parallel to flow and therefore parallel to the strings at the high shear rate, $\dot{\gamma} > \dot{\gamma}_a$. The elongated two-point pattern at the large q-region superposed on the streak pattern at the small q-region suggests that the strings may have internal structures composed of domains rich in polymers (dark oblates) and poor in polymers (gray region) as schematically illustrated in part d′ (an enlarged model of the strings in part d). At $\dot{\gamma} > \dot{\gamma}_a$ these domains are aligned in a row parallel to the flow axis, forming the strings, but they are not aligned in a row at $\dot{\gamma}_c < \dot{\gamma} < \dot{\gamma}_a$, as schematically shown in the enlarged model of part c (part c′).

The PS used are not crystallizable polymers, and consequently they were not crystallized under the shear flow. This result suggests that the strings formed at high shear rates may eventually result in crystallization into row nuclei, when polymers are crystallizable, as we reported elsewhere.[23,29]

V. Summaries

We can classify the shear rate dependence of dichroism and birefringence for high molecular weight semidilute polystyrene solutions under the shear flow in the same manner as those of light scattering and rheological behavior in terms of the critical shear rate. It is believed that the change in the sign of the dichroism is due to the shear-induced formation of stringlike structures oriented parallel to flow and that the change of birefringence associated with the string formation is due to the orientation PS chains in the strings with their end-to-end vectors parallel to flow and axes of the strings.

Acknowledgment. This work was supported in part by a Grant-in-aid for Scientific Research on Priority Areas “Cooperative Phenomena in Complex Fluids” (07236103) addressed to T.H. and by a Grant-in-aid for Encouragement of Young Scientists-A (00062753) addressed to T.K., both from the Ministry of Education, Science, Sports, and Culture, Japan.

References and Notes

(1) *Flow-Induced Structure in Polymers*; Nakatani, A. I.; Dadmun, M. D., Eds.; ACS Symposium Series 597; American Chemical Society: Washington, DC, 1995.
(2) Ver Strate, G.; Philippoff, W. J. *J. Polym. Sci., Polym. Lett. Ed.* **1974**, *12*, 267.
(3) Wolf, B. A. *Makromol. Chem., Rapid Commun.* **1980**, *1*, 231.
(4) Rangel-Nafaile, C.; Metzner, A. B.; Wissbrun, K. F. *Macromolecules* **1984**, *17*, 1187.
(5) Helfand, E.; Fredrickson, G. H. *Phys. Rev. Lett.* **1989**, *62*, 2468.
(6) Onuki, A. *Phys. Rev. Lett.* **1989**, *62*, 2472.
(7) Onuki, A. *J. Phys. Soc. Jpn.* **1990**, *59*, 3427.
(8) Hashimoto, T.; Takebe, T.; Fujioka, K. In *Dynamics and Patterns in Complex Fluids*; Onuki, A., Kawasaki, K., Eds.; Springer: Heidelberg, Germany, 1990; p 86.
(9) Hashimoto, T.; Fujioka, K. *J. Phys. Soc. Jpn.* **1991**, *60*, 356.
(10) Milner, S. T. *Phys. Rev. Lett.* **1991**, *66*, 1477.
(11) Wu, X.-L.; Pine, D. J.; Dixon, P. K. *Phys. Rev. Lett.* **1991**, *66*, 2408.
(12) Yanase, H.; Moldenaers, P.; Mewis, J.; Abetz, V.; van Egmond, J.; Fuller, G. G. *Rheol. Acta* **1991**, *30*.
(13) Larson, R. G. *Rheol. Acta* **1992**, *31*, 497.
(14) Doi, M.; Onuki, A. *J. Phys. 2 Fr.* **1992**, *2*, 1631.
(15) Hashimoto, T.; Kume, T. *J. Phys. Soc. Jpn.* **1992**, *61*, 1839.
(16) Dixon, P. K.; Pine, D. J.; Wu, X.-L. *Phys. Rev. Lett.* **1992**, *68*, 2239.
(17) van Egmond, J. W.; Werner, D. E.; Fuller, G. G. *J. Chem. Phys.* **1992**, *96*, 7742.
(18) Mavrantzas, V. G.; Beris, A. N. *Phys. Rev. Lett.* **1992**, *69*, 273.
(19) Moldenaers, P.; Yanase, H.; Mewis, J.; Fuller, G. G.; Lee, C.-S.; Magda, J. J. *Rheol. Acta* **1993**, *32*, 1.
(20) van Egmond, J. W.; Fuller, G. G. *Macromolecules* **1993**, *26*, 7182.
(21) Moses, E.; Kume, T.; Hashimoto, T. *Phys. Rev. Lett.* **1994**, *72*, 2037.
(22) Boué, F.; Lindner, P. *Europhys. Lett.* **1994**, *25*, 421.
(23) Murase, H.; Ohta, Y.; Mizukami, T.; Yasuda, H.; Kume, T.; Hashimoto, T. *ISF '94*; Yokohama, Japan, 1994; p 286.
(24) Fuller, G. *Optical Rheometry of Complex Fluids*; Oxford University Press: New York, 1995.
(25) Kume, T.; Asakawa, K.; Moses, E.; Matsuzaka, K.; Hashimoto, T. *Acta Polym.* **1995**, *46*, 79.
(26) Fuller, G.; van Egmond, J.; Wirtz, D.; Peuvrel-Disdier, E.; Wheeler, E.; Takahashi, T. In *Flow-Induced Structure in Polymers*; Nakatani, A. I., Dadmun, M. D., Eds.; American Chemical Society: Washington, DC, 1995; p 22.
(27) Kume, T.; Hashimoto, T. In *Flow-Induced Structure in Polymers*; Nakatani, A. I., Dadmun, M. D., Eds.; American Chemical Society: Washington, DC, 1995; p 35.
(28) Hashimoto, T.; Matsuzaka, K.; Moses, E.; Onuki, A. *Phys. Rev. Lett.* **1995**, *74*, 126.
(29) Murase, H.; Kume, T.; Hashimoto, T.; Ohta, Y.; Mizukami, T. *Macromolecules* **1995**, *28*, 7724.
(30) Murase, H.; Kume, T.; Hashimoto, T.; Ohta, Y.; Mizukami, T. *Macromol. Symp.* **1996**, *104*, 159.
(31) Migler, K.; Liu, C.; Pine, D. J. *Macromolecules* **1996**, *29*, 1422.
(32) Takahashi, T.; Fuller, G. *Rheol. Acta* **1996**, *35*, 297.
(33) Kume, T.; Hattori, T.; Hashimoto, T. *Macromolecules* **1997**, *30*, 427.
(34) Park, J. O.; Berry, G. C. *Macromolecules* **1989**, *22*, 3022.
(35) Hashimoto, T.; Takebe, T.; Suehiro, S. *Polym. J.* **1986**, *18*, 123.
(36) The structural characteristic was presented more clearly in Figure 11d of ref 30.

MA9705984